

# Spatial structure of the pair wave function and the density correlation functions throughout the 2D BEC-BCS crossover

J.C. Obeso-Jureidini and V. Romero-Rochín

*Instituto de Física, Universidad Nacional Autónoma de México*

*Apartado Postal 20-364, 01000 Cd. México, Mexico*

(Dated: November 9, 2021)

## Abstract

The spatial structure of a two-dimensional homogeneous mixture of fermionic atoms in two hyperfine states is analyzed throughout the BEC-BCS crossover. Within the BCS-Leggett mean-field model we consider three functions: the pair wave function and the density correlation functions between atoms of the same and of different hyperfine states. For the correlation functions we derive analytical expressions which allow to unveil the rich spatial structure of the superfluid. Mainly, we are able to study the large-distance behavior of the three functions, which exhibits an exponential decay and a well-defined oscillatory behavior. We report closed-form expressions for the correlation lengths and mean pair radius. Differences and similarities emerge when comparing with the three dimensional case. Particularly, we find an invariant expression for the exponential decay length.

## I. INTRODUCTION

Experimental advances in ultracold atoms have surprised the community with the creation of physical systems with unprecedented control over their properties [1–5]. An example is the achievement of spatial confinement to two dimensions (2D) [2, 6–8], offering an exceptional opportunity for testing theoretical models against experiments. Such is the case of the 2D BEC-BCS crossover, implemented by Miyake [9], and Randeria, Duan, and Shieh [10]. Their mean-field model, which concerns us, consists of a homogeneous balanced mixture of two fermionic species with a renormalized contact interaction between unlike particles, similarly to the three dimensional model of Leggett [11] and Eagles [12]. Depending on the strength of the interactions, different many-body states can be obtained. For weakly attractive interactions a gas of Cooper pairs is obtained, corresponding to the Bardeen-Cooper-Schrieffer regime (BCS) [13]. On the other hand, for strongly attractive interactions a gas of diatomic molecules is generated, which condenses at zero temperature, corresponding to a Bose-Einstein condensation state (BEC). However, for intermediate strengths, the many-body states form a continuum that connects both regimes, known as the crossover region. An important question about the BEC-BCS crossover concerns the description of the pairing mechanism of unlike particles, giving rise to BCS-superfluidity and Bose-Einstein condensation [2, 4]. To address this question we analyze the spatial structure of the gas within the 2D mean-field BCS-Leggett model aforementioned [9, 10]. The spatial structure can be extracted from the analysis of three functions: the correlation function between same species, the correlation function between different species, and the variational pair wave function.

The main contribution of this article is to present analytical expressions for the two correlation functions, an important result that allows to obtain a detailed picture of the behavior of the gas throughout the crossover. For the pair wave function, while we are unable to find an analytical expression for all values of the interaction, we do find its large distance behavior, and we analyze it with the aid of numerical calculations. Also, we report closed-form expressions for the correlation lengths and mean pair radius defined as the respective second moment for each distribution. Similarly to the 3D case [14, 15], we can analyze the pairing phenomenon throughout the crossover. In the BCS limit, correlated pairs of unlike

particles can have multiple sizes, particularly of macroscopic order, while Pauli-blocking correlations prevent two like particles to be found near each other. In the BEC limit the sizes of correlated pairs of unlike particles tend to be small, while Pauli-blocking correlations become negligible. Further, with our analytical expressions, we are able to study the large distance behavior of the correlation functions and the pair wave function. We find that the three functions exhibit an exponential decay and a well-defined oscillatory behavior. The exponential decay is characterized by an exponential decay length, which turns to be dependent of the two-body physics used to renormalize the interaction strength. The spatial oscillation frequency turns out to be constant throughout the crossover, being equal to the Fermi wave number. The large distance behavior found in 2D can be contrasted with the behavior found in 3D [14]. Particularly, we find that the exponential decay length has the same expression in 2D and in 3D, when expressed in terms of thermodynamic variables.

The article is organized as follows. In section II we give a brief review of the two-body scattering problem used to renormalize the interaction strength in the many-body problem. In section III, we introduce the 2D mean-field BCS-Leggett model and discuss the relevance of the two-body physics. In section IV we present the main study of the two-body distributions. Analytical expressions for both correlation functions are reported. We analyze the large-distance behavior of the three functions by studying the spatial oscillation and the exponential decay length. Lastly, we report closed-form expressions for the correlation lengths and the mean pair radius. Finally, in section V we present our discussions and final remarks.

## II. TWO-BODY SCATTERING PROPERTIES FOR THE MANY-BODY PROBLEM

In this section we consider the problem of scattering of equal mass particles from a non-divergent short-range central potential  $U(r)$ . The low energy limit of the  $T$  matrix is given by [10, 16–18]

$$T(2E) \approx \frac{4\hbar^2}{m} \left[ \frac{1}{\ln(E_a/2E)/\pi + i} \right]. \quad (1)$$

where  $m$  is the mass of a particle and  $E = \hbar^2 k^2 / 2m$  is half the energy of relative motion [10, 16]. The quantity  $E_a$  is the approximate energy at which a scattering resonance occurs [10, 16–18]. However, when the potential  $U(r)$  does not change sign in the interval  $[0, r_0]$ , where  $r_0$  is the range of the potential, the energy  $E_a$  is also a good approximation of the absolute value of an ever-present bound state energy  $E_{\text{bound}}$  [16]. In Fig. 1 we show a comparison between the energy of the  $s$ -wave resonance  $E_{\text{res}}$  [17, 18], the absolute value of the bound state energy  $|E_{\text{bound}}|$ , and the energy  $E_a$ , for a shallow-enough circular potential (analogous of the spherical well in 3D) of depth  $-U_0$  and radius  $r_0$ . It is seen that the three energies differ when we increase the depth  $U_0$  or the radius  $r_0$ .

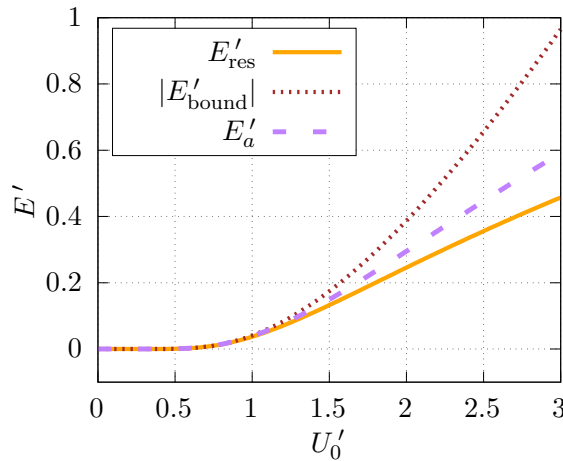


FIG. 1. (Color online) Comparison between the bound state energy  $|E_{\text{bound}}|$ , shown with a dotted line (brown); the exact  $s$ -wave resonance energy  $E_{\text{res}}$  [17], solid curve (orange); and the approximate energy  $E_a$ , shown with a dashed line (purple), for the circular potential illustrated in the inset. The depth of the potential is given by  $-U_0$  and the radius is  $r_0$ . The primed variables correspond to dimensionless quantities, using  $m = \hbar = r_0 = 1$ .

The contact interaction corresponds to a Dirac-delta function,

$$U(\mathbf{r}) = g\delta^{(2)}(\mathbf{r}), \quad (2)$$

where  $g < 0$  is the interaction strength. Iterating the  $T$  matrix in the Lippmann-Schwinger equation we can find an expression for the interaction strength in terms of the low energy

limit of the  $T$  matrix (1) and a divergent term [3, 4, 10, 19, 20]:

$$\begin{aligned} \frac{1}{g(\Lambda)} &= \frac{1}{T(2E)} + \frac{1}{A} \sum_{\mathbf{k}''}^{\Lambda} \frac{1}{2(E - \varepsilon_{\mathbf{k}''} + i\delta)} \\ &= \frac{m}{4\pi\hbar^2} \ln\left(\frac{E_a}{2\Lambda}\right) \end{aligned} \quad (3)$$

where  $A \rightarrow \infty$  is an auxiliary area and we introduced a cutoff  $\Lambda$ . In the last equality we took the limit  $\delta \rightarrow 0^+$  and neglected smaller terms than the cutoff  $\Lambda$ . The divergence associated with the limit  $\Lambda \rightarrow \infty$  is useful to cancel out a divergence that arises in the many-body problem, as shown below in section III. Equation (3) can also be obtained from the bound state problem of the contact interaction, allowing to identify  $E_a = |E_{\text{bound}}|$  [9, 21–23].

### III. MEAN-FIELD APPROACH OF THE ATTRACTIVE FERMI GAS IN THE 2D BEC-BCS CROSSOVER

We consider a balanced gas mixture of fermionic atoms of mass  $m$  in two hyperfine states, interacting via a contact potential. In the following we will treat these states as spins with the notation  $\sigma = \uparrow, \downarrow$ . In the low-density and low-energy limit we consider the grand potential  $\hat{\Omega} = \hat{H} - \mu\hat{N}$  given by

$$\hat{\Omega} = \sum_{\mathbf{k}, \sigma} (\epsilon_{\mathbf{k}} - \mu) c_{\mathbf{k}\sigma}^\dagger c_{\mathbf{k}\sigma} + \frac{g}{A} \sum_{\mathbf{k}_1 \mathbf{k}_2} c_{\mathbf{k}_1 \uparrow}^\dagger c_{-\mathbf{k}_1 \downarrow}^\dagger c_{-\mathbf{k}_2 \downarrow} c_{\mathbf{k}_2 \uparrow}, \quad (4)$$

where  $\epsilon_{\mathbf{k}} = \hbar^2 k^2 / 2m$ ,  $g$  is the interaction strength and  $A$  is the area of the sample. The operator  $c_{\mathbf{k}\sigma}^\dagger$  creates a fermionic atom with momentum  $\mathbf{k}$  and spin  $\sigma$ , the sums are over all wave vectors  $\mathbf{k}$ . As in 3D, we can estimate the ground state energy by means of the BCS-Leggett variational method [11], or the mean-field method [9, 10, 22, 24]. We will focus on the variational method which introduces the BCS wave function [13]

$$|\Psi_{\text{BCS}}\rangle = \prod_{\mathbf{k}} (u_{\mathbf{k}} + v_{\mathbf{k}} c_{\mathbf{k}\uparrow}^\dagger c_{-\mathbf{k}\downarrow}^\dagger) |0\rangle, \quad (5)$$

where the variational parameters satisfy the normalization condition  $|u_{\mathbf{k}}|^2 + |v_{\mathbf{k}}|^2 = 1$ . A thermodynamic quantity that arises naturally from the minimization procedure is the gap  $\Delta$  [25], which is related directly to the interaction properties of the fermions by means of the gap equation

$$1 = -\frac{g(\Lambda)}{2A} \sum_{\mathbf{k}} \frac{1}{\sqrt{(\epsilon_{\mathbf{k}} - \mu)^2 + \Delta^2}}, \quad (6)$$

where we introduced a cutoff  $\Lambda$ . As usual, the number equation is given by

$$n = \frac{1}{A} \sum_{\mathbf{k}} \left( 1 - \frac{\epsilon_k - \mu}{\sqrt{(\epsilon_k - \mu)^2 + \Delta^2}} \right), \quad (7)$$

where  $n = N/A$  is the particle density. Also, the variational parameters can be expressed in terms of the gap and the chemical potential:

$$\begin{Bmatrix} u_k^2 \\ v_k^2 \end{Bmatrix} = \frac{1}{2} \left[ 1 \pm \frac{\epsilon_k - \mu}{\sqrt{(\epsilon_k - \mu)^2 + \Delta^2}} \right]. \quad (8)$$

Hence, (6) and (7) have to be solved simultaneously. Before proceeding, let us point out that the energy per area of the system can be calculated directly [19, 26]

$$\begin{aligned} \frac{E_0}{A} &= \frac{1}{A} \sum_{\mathbf{k}} \left( \epsilon_k - \frac{\epsilon_k(\epsilon_k - \mu) - \Delta^2/2}{\sqrt{(\epsilon_k - \mu)^2 + \Delta^2}} \right) \\ &= \frac{m}{4\pi\hbar^2} \left( 3\mu\sqrt{\mu^2 + \Delta^2} + \mu^2 - \frac{\Delta^2}{2} \right). \end{aligned} \quad (9)$$

This expression can be obtained without renormalization, in a similar way as in 3D [14, 15]. Returning to the gap equation (6), notice it exhibits an ultraviolet divergence associated to the contact interaction, that can be removed using equation (3) [9, 10, 22]. Thus we obtain the condition [7]:

$$E_a = \sqrt{\mu^2 + \Delta^2} - \mu. \quad (10)$$

This is a curious result because it coincides with the threshold energy required to create a quasiparticle by exciting an atom to a third state with negligible momentum transfer, which we denote by [3, 7, 27]

$$\epsilon_{\text{spec}} = \sqrt{\mu^2 + \Delta^2} - \mu. \quad (11)$$

From the number equation we get [9, 10]

$$2\epsilon_F = \mu + \sqrt{\mu^2 + \Delta^2}, \quad (12)$$

where  $\epsilon_F = \hbar^2 k_F^2 / (2m)$  is the Fermi energy and  $k_F = \sqrt{2\pi n}$  is the Fermi wave number. Equations (10) and (12) can be solved to find that the chemical potential is the Fermi energy minus half the binding energy of the contact interaction [9, 10],

$$\mu = \epsilon_F - \frac{E_a}{2}, \quad (13)$$

while the gap is proportional to the geometric mean of the Fermi energy  $\epsilon_F$  and the energy of resonance  $E_a$  [9, 10],

$$\Delta = \sqrt{2\epsilon_F E_a}. \quad (14)$$

The BCS limit corresponds to values of  $E_a$  near zero, while the BEC limit corresponds to  $E_a$  going to infinity [9, 10]. With equations (10) and (12) the ground state energy (9) can be written in terms of the resonance energy  $E_a$  [10]. Then we can calculate a relevant quantity for our purposes, which is the binding energy per pair  $\epsilon_b$ . We find [7, 10]

$$\epsilon_b = \frac{2}{N} (E_F - E_0) = E_a. \quad (15)$$

This equality marks a difference with the 3D case, where  $\epsilon_b^{3D} \neq \epsilon_{\text{spec}}^{3D}$  [14, 15], see equations (10) and (11). Hence, the resonance energy  $E_a$  acquires many physical properties: It is the energy where a scattering resonance occurs; it is the absolute value of the bound state energy of the delta potential; it is a parameter to tune between the BEC and BCS regimes; it is the binding energy per pair  $\epsilon_b$  of the many-body system and it is the threshold energy required to create a quasiparticle with minimum momentum transfer by exciting an atom to a third state  $\epsilon_{\text{spec}}$ . All these binding properties suggest that the correlation functions will be endowed with an exponential decay behavior determined by  $E_a$ , as will be shown in the next section.

#### IV. PAIR WAVE FUNCTION AND DENSITY CORRELATION FUNCTIONS

The two-body functions we analyze in this study are relevant for understanding the spatial structure of the gas and have been a subject of interest for ultracold gases [3, 4, 28–30]. For instance, the density correlation functions give physical information about the probability of finding two types of particle at different spatial points. Also, they measure the relation between density fluctuations at different points. On the other hand, the spatial projection of the BCS state (5) to a fixed number of particles state allows us to identify the unnormalized pair wave function [11]:

$$\phi_{\text{BCS}}(\mathbf{r}) = \frac{1}{(2\pi)^2} \int d^2k e^{i\mathbf{k}\cdot\mathbf{r}} \frac{v_k}{u_k}. \quad (16)$$

In concrete, we propose to study the density correlation functions between spins [4, 28]

$$G_{\sigma\sigma'}(\mathbf{x}, \mathbf{x}') = \langle \hat{n}_\sigma(\mathbf{x}) \hat{n}_{\sigma'}(\mathbf{x}') \rangle - \langle \hat{n}_\sigma(\mathbf{x}) \rangle \langle \hat{n}_{\sigma'}(\mathbf{x}') \rangle, \quad (17)$$

where  $\sigma$  and  $\sigma'$  are spin labels which can take the values  $\uparrow$  or  $\downarrow$ . We have introduced the particle density operator at point  $\mathbf{x}$  of spin  $\sigma$  given by  $\hat{n}_\sigma(\mathbf{x}) = \hat{\psi}_\sigma^\dagger(\mathbf{x})\hat{\psi}_\sigma(\mathbf{x})$ , where

$$\hat{\psi}_\sigma(\mathbf{x}) = \frac{1}{\sqrt{A}} \sum_{\mathbf{k}} e^{i\mathbf{k}\cdot\mathbf{x}} c_{\mathbf{k}\sigma} \quad (18)$$

are the usual field operators. The equal population property  $N_\uparrow = N_\downarrow$  allows us to equal the labels as  $\uparrow\uparrow = \downarrow\downarrow$  and  $\uparrow\downarrow = \downarrow\uparrow$ . Before proceeding, let us point out that for the free gas the correlation functions can be readily calculated, as in 3D [28, 29, 31],

$$G_{\uparrow\uparrow}^{\text{free}}(\mathbf{x}, \mathbf{x}') = \frac{n}{2} \delta^{(2)}(\mathbf{x} - \mathbf{x}') - \left[ n \frac{J_1(k_F|\mathbf{x} - \mathbf{x}'|)}{k_F|\mathbf{x} - \mathbf{x}'|} \right]^2, \quad (19)$$

where  $J_1$  is a Bessel function of the first kind of order one. Similar to the 3D case we have

$$G_{\uparrow\downarrow}^{\text{free}}(\mathbf{x}, \mathbf{x}') = 0. \quad (20)$$

In the interacting system the correlation function  $G_{\uparrow\downarrow}(\mathbf{x}, \mathbf{x}')$  will show a richer structure, owing to the interactions between opposite spins. As the system under consideration is homogeneous and isotropic, the correlation functions depend only on the relative position  $\mathbf{r} = \mathbf{x} - \mathbf{x}'$ . Thus, the correlation functions are given by

$$G_{\uparrow\downarrow}(\mathbf{r}) = |g_{\uparrow\downarrow}(\mathbf{r})|^2, \quad (21)$$

and

$$G_{\uparrow\uparrow}(\mathbf{r}) = \frac{n}{2} \delta^{(2)}(\mathbf{r}) - |g_{\uparrow\uparrow}(\mathbf{r})|^2 \quad (22)$$

where we have defined

$$g_{\uparrow\downarrow}(\mathbf{r}) = \frac{1}{(2\pi)^2} \int d^2k e^{i\mathbf{k}\cdot\mathbf{r}} u_k v_k. \quad (23)$$

and

$$g_{\uparrow\uparrow}(\mathbf{r}) = \frac{1}{(2\pi)^2} \int d^2k e^{i\mathbf{k}\cdot\mathbf{r}} v_k^2 \quad (24)$$

Until now the expressions have been similar to the 3D system [4, 14, 29]. However, we have to calculate two-dimensional Fourier transforms:

$$f(\mathbf{r}) = \int d^2k e^{i\mathbf{k}\cdot\mathbf{r}} \mathcal{F}(\mathbf{k}), \quad (25)$$

where  $\mathcal{F}(\mathbf{k})$  can be  $v_k/u_k$ ,  $u_k v_k$  or  $v_k^2$ . For the 3D system the angular integrals can be simply evaluated and we can complete a one-dimensional Fourier transform. Instead, in the 2D system, performing the angular integral leads us to a Hankel transform:

$$f(r) = 2\pi \int_0^\infty dk k \mathcal{F}(k) J_0(kr), \quad (26)$$

where we used  $f(\mathbf{r}) = f(r)$ ,  $r = |\mathbf{r}|$ , and we identified the integral representation of the Bessel function of the first kind of order zero [31]:

$$J_0(kr) = \frac{1}{2\pi} \int_0^{2\pi} d\theta e^{ikr \cos \theta}. \quad (27)$$

For the correlation functions, their respective integrals in equation (26) can be calculated analytically. The expressions are:

$$g_{\uparrow\downarrow}(r) = \frac{m\Delta}{2\pi\hbar^2} J_0(k_F r) K_0\left(\frac{r}{\sqrt{2}\chi_b}\right), \quad (28)$$

and

$$g_{\uparrow\uparrow}(r) = \frac{m\Delta}{2\pi\hbar^2} J_1(k_F r) K_1\left(\frac{r}{\sqrt{2}\chi_b}\right), \quad (29)$$

where, for comparison with the 3D results [14], we defined

$$\chi_b = \left(\frac{\hbar^2}{2m\epsilon_b}\right)^{1/2}. \quad (30)$$

Later we will argue that  $\chi_b$  is the exponential decay length. For the 2D system  $\epsilon_b = \epsilon_{\text{spec}} = E_a$ , as was discussed in Section III, see equation (11). Equations (28) and (29) can be verified by calculating their inverse Fourier transforms which give  $u_k v_k$  and  $v_k^2$ , respectively [32, 33]. The details of this procedure are given in Appendix A. For the pair wave function  $\phi_{\text{BCS}}(r)$  we were unable to find an analytical expression for all values of  $r$ . However, we will present a theoretical and numerical analysis of its large-distance behavior. Nevertheless, we can evaluate numerically equation (26) with  $\mathcal{F}(k) = v_k/u_k$ , a difficult task due to the Bessel function  $J_0(kr)$  as it oscillates and decreases slowly as  $kr \rightarrow \infty$ .

In Fig. 2 the correlation functions and the pair wave function can be seen at different points of the crossover. In the BCS limit,  $E_a \rightarrow 0$ , corresponding to Fig. 2 (a), the three functions show an algebraic decay at short distances. For instance,  $G_{\uparrow\uparrow}(r)$  behaves like the one of the non-interacting system, shown in equation (19), a similar observation was made in 3D [29]. The BCS limit of the pair wave function is

$$\phi_{\text{BCS}}(r) \approx \frac{2\varepsilon_F}{\pi\Delta} k_F^2 \frac{J_2(k_F r)}{(k_F r)^2}. \quad (31)$$

The BCS limit of  $G_{\uparrow\downarrow}(r)$  has an algebraic decay at short distances and a singularity at  $r = 0$ , showing that correlated pairs can have a great variety of sizes [14]. As we move to the BEC

side, increasing  $E_a$ , the correlation functions and the pair wave function get localized, as can be seen in Fig. 2 (b), (c) and (d), indicating the formation of bosonic molecules and the gradual lost of Pauli-blocking correlations [14]. Comparing the behavior of  $v_k u_k$  and  $v_k / u_k$  on the deep BEC side,  $-\mu \gg \Delta$ , we expect the pair wave function  $\phi_{\text{BCS}}(r)$  to approach the function  $g_{\uparrow\downarrow}(r)$ , just as in the 3D system [14, 15],

$$\phi_{\text{BCS}}(r) \approx g_{\uparrow\downarrow}(r). \quad (32)$$

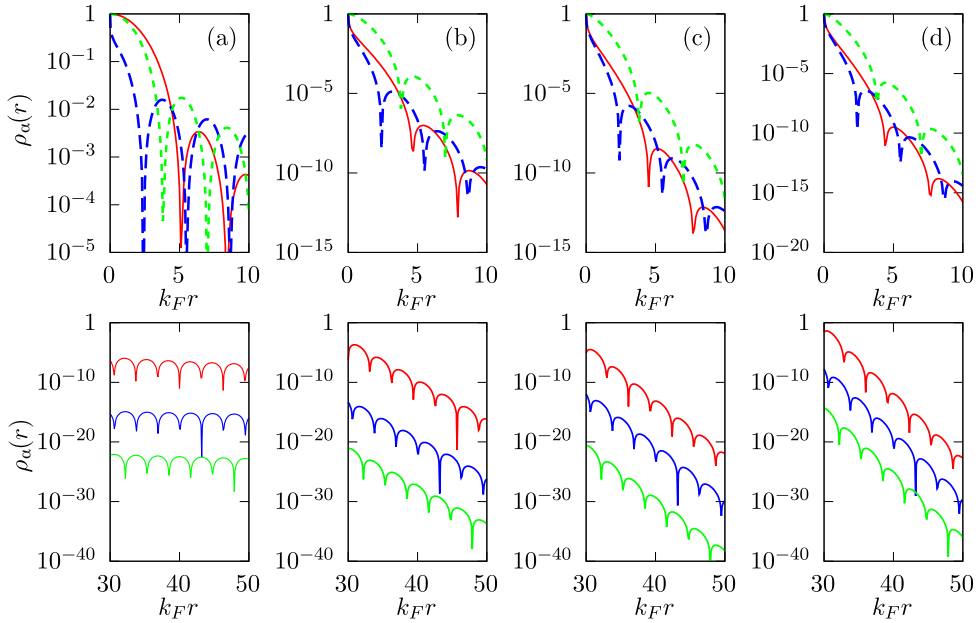


FIG. 2. (Color online) Correlation functions and pair wave function throughout the crossover. Each column corresponds to different points of the crossover, (a)  $E_a/\epsilon_F = 0.0001$  (BCS side), (b)  $E_a/\epsilon_F = 1$ , (c)  $E_a/\epsilon_F = 2$  (d)  $E_a/\epsilon_F = 3$  (BEC side). In the upper panel the solid line (red) corresponds to  $\rho_\alpha(r) = |\phi_{\text{BCS}}(r)|^2$ , the long dashed line (blue) to  $\rho_\alpha(r) = G_{\uparrow\downarrow}(r)$  and the short dashed line (green) corresponds to  $\rho_\alpha(r) = G_{\uparrow\uparrow}(r)$ . They are plotted with arbitrary normalization. The lower panel shows the behavior at large distances, where the upper curves correspond to  $|\phi_{\text{BCS}}(r)|^2$ , the middle ones to  $G_{\uparrow\downarrow}(r)$  and the lower curves to  $-G_{\uparrow\uparrow}(r)$ . In all the panels we removed the delta function of  $G_{\uparrow\uparrow}(r)$ .

Observation of the lower panel of Fig. 2 suggests a common characterization of the large-distance behavior of the distributions  $|\phi_{\text{BCS}}(r)|^2$ ,  $|g_{\uparrow\downarrow}(r)|^2$  and  $|g_{\uparrow\uparrow}(r)|^2$ . That is, for large

distances  $k_F r \gg 1$  these distribution functions can be written in the form

$$\rho_\alpha(r) \approx \frac{\text{const}}{r^2} e^{-\frac{\sqrt{2}r}{\chi_\alpha}} \mathcal{P}_\alpha(\kappa_\alpha r + \varphi_\alpha), \quad (33)$$

where  $\alpha = \text{BCS}, \uparrow\downarrow, \uparrow\uparrow$  and we have introduced a periodic function  $\mathcal{P}_\alpha(\kappa_\alpha r + \varphi_\alpha)$  with wave length  $2\pi/\kappa_\alpha$  and phase  $\varphi_\alpha$ . In fact, for the correlation functions, the functional form for large distances can be identified using well-known properties of the Bessel functions [33], as

$$|g_{\uparrow\downarrow}(r)|^2 \approx \frac{\text{const}}{r^2} e^{-\frac{\sqrt{2}r}{\chi_b}} \cos^2\left(k_F r - \frac{\pi}{4}\right), \quad (34)$$

$$|g_{\uparrow\uparrow}(r)|^2 \approx \frac{\text{const}}{r^2} e^{-\frac{\sqrt{2}r}{\chi_b}} \cos^2\left(k_F r - \frac{3\pi}{4}\right). \quad (35)$$

### A. Characteristic wave numbers and phases

From equations (34) and (35), we can conclude that the wave vectors of the correlation functions are  $\kappa_{\uparrow\downarrow} = k_F$  and  $\kappa_{\uparrow\uparrow} = k_F$ . For the pair wave function we also determined numerically that  $\kappa_{\text{BCS}} = k_F$ , as shown in Fig. 3 (a). This was done finding the average distance between consecutive nodes, like the ones shown in the lower panel of Fig 2, for values of  $E_a/\epsilon_F$  between 0.0001 and 8, using points separated by a distance  $k_F \delta r = 0.1$ . Hence, we can see a difference with the 3D system, where the wave vectors are similar to  $k_F$  in the BCS limit and decrease as we move to the BEC side [14], while in the 2D system they remain constant. Thus the wave vectors  $\kappa_\alpha$  of equation (33) are given by

$$\kappa_\alpha(E_a) = k_F, \quad (36)$$

for  $\alpha = \text{BCS}, \uparrow\downarrow, \uparrow\uparrow$ . Therefore, the density determines the large-distance oscillatory behavior throughout the crossover.

Regarding the phases, it is appropriate to study the phase differences between distributions. With equations (34) and (35) it is readily proven that the phase difference between the correlation functions is constant throughout the crossover:

$$\varphi_{\uparrow\uparrow} - \varphi_{\uparrow\downarrow} = \frac{\pi}{2} + m\pi, \quad (37)$$

where  $m$  is an integer. The phase differences between the pair wave function and the correlation functions are shown in Fig. 3. As expected from equations (31) and (34), on the BCS side the nodes of the pair wave function  $\phi_{\text{BCS}}(r)$  are near the nodes of  $g_{\uparrow\downarrow}(r)$ . Moving

towards the BEC limit, after the chemical potential becomes negative, the nodes of the pair wave function approach the nodes of  $g_{\uparrow\uparrow}(r)$ . On the deep BEC limit the nodes of the pair wave function should approach the ones of  $g_{\uparrow\downarrow}(r)$  again.

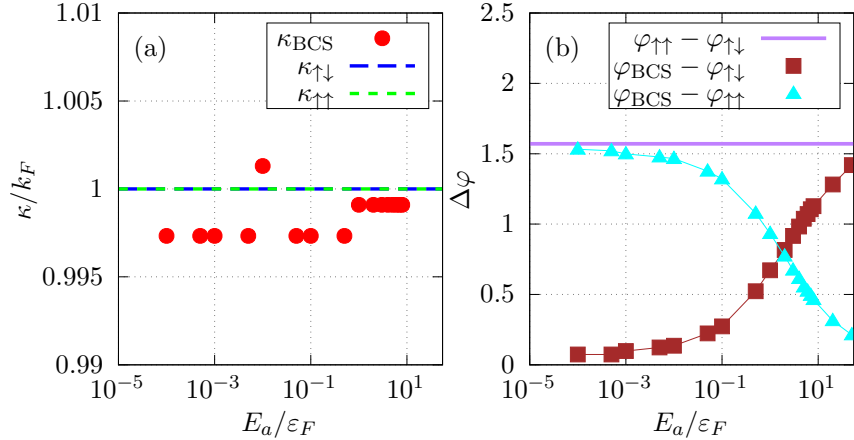


FIG. 3. (Color online) (a) Large-distance wave vectors  $\kappa_{BCS}$ ,  $\kappa_{\uparrow\downarrow}$ ,  $\kappa_{\uparrow\uparrow}$  scaled with the Fermi wave number  $k_F$ , see equation (33). The dots (red) correspond to numerical calculations of  $\kappa_{BCS}$ . The behavior  $\kappa_{\uparrow\downarrow} = \kappa_{\uparrow\uparrow} = k_F$  was obtained analytically. (b) Phase differences between the pair wave function (BCS) and the density correlation functions ( $\uparrow\uparrow$ ,  $\uparrow\downarrow$ ). The phase difference  $\varphi_{\uparrow\uparrow} - \varphi_{\uparrow\downarrow}$  is a theoretical result, while the other two were obtained numerically (the lines are guides to the eye). Notice the logarithmic scale of  $E_a/\epsilon_F$  in both graphs.

## B. Exponential decay lengths

Now we focus on the exponential decay behaviors, shown in the lower panel of Fig. 2. For the correlation functions this behavior can be extracted quantitatively comparing equations (34) and (35) with equation (33). It is concluded that their exponential decay lengths are, both,  $\chi_{\uparrow\downarrow} = \chi_{\uparrow\uparrow} = \chi_b$ . For the pair wave function  $\phi_{BCS}(r)$  we can extract its behavior by analyzing equation (26) and from numerical calculations. An interesting procedure is to extend the integral of equation (26) to the complex plane to close an integration contour, as was done in the 3D system [14]. This allows to find an integral representation of the Hankel transform (26) that might be easier to compute. Though, as we are interested in the

large-distance behavior, we can approximate the Bessel function  $J_0(kr)$ , for  $kr \gg 1$ , by [34]

$$J_0(kr) \approx \frac{e^{i(kr-\pi/4)} + e^{-i(kr-\pi/4)}}{\sqrt{2\pi kr}}. \quad (38)$$

As in 3D, the square root  $[(\epsilon_k - \mu)^2 + \Delta^2]^{1/2}$  that belongs to the variational parameters (8) gives rise to four branch cuts. By closing an adequate contour on the complex plane we can obtain an integral of an exponentially decreasing function. Details of this mathematical procedure are given in Appendix B. Then, the large-distance behavior of  $\phi_{\text{BCS}}(r)$  is approximated by

$$\begin{aligned} \phi_{\text{BCS}}(r) \propto & \frac{1}{\sqrt{k_F r}} \int_{\tau_0}^{\infty} e^{-\tau k_F r} \left( \frac{2\tau^2 + \tilde{\mu}}{\tilde{\Delta}} \right)^{1/4} \left[ \cos \left( \sqrt{\frac{\tau^2 + \tilde{\mu}}{\tilde{\Delta}}} \right) \left( \cos(\theta(\tau)/2) - \frac{\tau \sin(\theta(\tau)/2)}{\sqrt{\tau^2 + \tilde{\mu}}} \right) \right. \\ & \left. + \sin \left( \sqrt{\frac{\tau^2 + \tilde{\mu}}{\tilde{\Delta}}} \right) \left( \frac{\tau \cos(\theta(\tau)/2)}{\sqrt{\tau^2 + \tilde{\mu}}} + \sin(\theta(\tau)/2) \right) \right] \left( \frac{\sqrt{4\tau^2(\tau^2 + \tilde{\mu}) - \tilde{\Delta}^2}}{\tilde{\Delta}} \right) d\tau, \end{aligned} \quad (39)$$

where  $\tau_0 = \{[(\tilde{\mu}^2 + \tilde{\Delta}^2)^{1/2} - \tilde{\mu}]/2\}^{1/2}$ ,  $\tilde{\mu} = \mu/\epsilon_F$ ,  $\tilde{\Delta} = \Delta/\epsilon_F$  and we have introduced the function

$$\theta(\tau) = \tan^{-1} \left( \frac{\sqrt{\tau^2 + \tilde{\mu}}}{\tau} \right). \quad (40)$$

The approximation of the Bessel function in equation (38) removes part of the structure, mainly the oscillations. Nevertheless, the main aspect to point out is that the integrand has an exponential factor  $\exp(-\tau k_F r)$ . This factor should persist after integration, but evaluated at  $\tau_0$ . Hence, we expect the Hankel transform of  $v_k/u_k$  to have an exponential decay behavior of the form

$$\phi_{\text{BCS}}(r) \propto \frac{e^{-r/\sqrt{2}\chi_b}}{\sqrt{r}}. \quad (41)$$

From this expression we can identify the exponential decay length  $\chi_{\text{BCS}} = \chi_b$ , as predicted. To reinforce this conclusion we calculated numerically the exponential decay length from the envelopes of the pair wave function, like the ones shown in the lower panel of Fig. 2. These numerical calculations correspond to the dots in Fig. 4 (a), showing good agreement with  $\chi_b$ , shown with long dashes in Fig. 4 (a). For the purpose of associating the exponential decay behavior with a pair binding property we define a *pair-binding* function:

$$|\Phi_b(r)|^2 = \frac{\text{const}}{r} e^{-\sqrt{2}r/\chi_b}, \quad (42)$$

where  $\chi_b$  is the exponential decay length defined in equation (30). This distribution has the large-distance asymptotic behavior of a bound state in a short-range central potential with zero angular momentum. Hence, the exponential decay length of the two-body bound state (42) remains as a characteristic length of the exponential decay behavior of the correlation functions and the pair wave function. Interestingly, the presence of a bound state throughout the crossover, as discussed in section II, determines the behavior of the correlation functions and the pair wave function.

Finally, it is of interest to compare with the 3D system. In Ref. [14] the 3D correlation functions and the pair wave function were obtained in terms of integrals, where the integrand has an exponential factor. Then we can argue again that this exponential must persist after integration, evaluated at the lower limit of the integral. Hence it can be concluded that the correlation functions  $G_{\uparrow\downarrow}^{3D}(r)$ ,  $G_{\uparrow\uparrow}^{3D}(r)$  and the pair wave function  $\phi_{BCS}^{3D}(r)$  in 3D show an exponential decay behavior at large distances of the form

$$\rho_{\alpha}^{3D}(r) \propto \frac{\text{const}}{r^2} \exp\left(-\frac{\sqrt{2}r}{\chi_{\text{spec}}^{3D}}\right) \mathcal{P}_{\alpha}^{3D}(r), \quad (43)$$

where  $\alpha = \text{BCS}, \uparrow\downarrow, \uparrow\uparrow$  and  $\mathcal{P}_{\alpha}^{3D}(r)$  are periodic functions of  $r$ . In this expression we have introduced

$$\chi_{\text{spec}}^{3D} = \left(\frac{\hbar^2}{2m \epsilon_{\text{spec}}^{3D}}\right)^{1/2}. \quad (44)$$

where  $\epsilon_{\text{spec}}^{3D}$  is defined as in equation (11) but with the corresponding chemical potential and gap of a 3D system. Therefore, the threshold energy  $\epsilon_{\text{spec}}$  strictly defined in terms of the gap  $\Delta$  and the chemical potential  $\mu$ , as in equation (11), provides the exponential decay length  $\chi_{\text{spec}}$  in 2D and in 3D, as shown by equations (30) and (44).

### C. Mean pair radius and correlation lengths

The exponential decay lengths are a property of the large-distance behavior of the distributions. However, if we are interested in a length that characterizes the global properties of the two-body distributions, it is adequate to consider their second moment:

$$\xi_{\alpha}^2 = \frac{|\int r^2 \rho_{\alpha}(r) d^2r|}{|\int \rho_{\alpha}(r) d^2r|}, \quad (45)$$

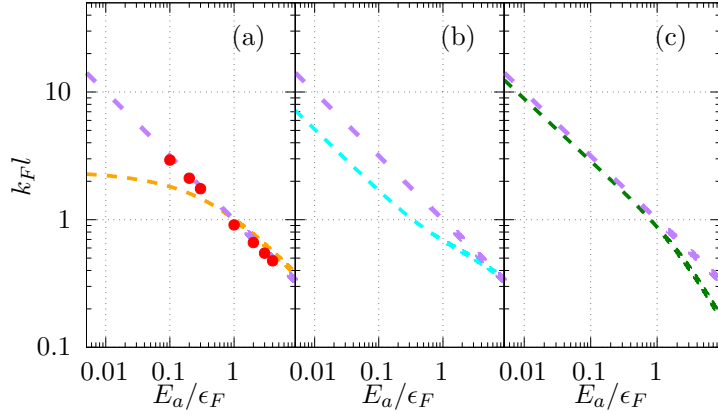


FIG. 4. (Color online) Characteristic lengths of (a) the pair wave function  $\phi_{BCS}(r)$  (16), (b) the correlation function of opposite spins  $G_{\uparrow\downarrow}(r)$  (21) and (c) the correlation function of parallel spins  $G_{\uparrow\uparrow}(r)$  (22). In each panel, the short dashes correspond to (a) the mean pair radius  $\xi_{BCS}$  and correlation lengths, (b)  $\xi_{\uparrow\downarrow}$  and (c)  $\xi_{\uparrow\uparrow}$ , see equation (45). In all panels the large dashes (purple) correspond to the exponential decay length  $\chi_b$ , shown in equation (30). The dots (red) in (a) are numerical calculations of the exponential decay length  $\chi_{BCS}$ , showing good agreement with  $\chi_b$ . The correlation length  $\xi_{\uparrow\downarrow}$  was reported in [10].

where  $\rho_\alpha(r) = |\phi_{BCS}(r)|^2, G_{\uparrow\downarrow}(r), G_{\uparrow\uparrow}(r)$ , see equations (16), (21), and (22). For the pair wave function  $\phi_{BCS}(r)$  we call  $\xi_{BCS}$  the mean pair radius, while the lengths  $\xi_{\uparrow\downarrow}$  and  $\xi_{\uparrow\uparrow}$  are called correlation lengths. The correlation length  $\xi_{\uparrow\downarrow}$  has been studied in several references [10, 21, 35, 36], here we include it for completeness. These lengths are calculated easier using the wave vector representation, as has been done for  $\xi_{\uparrow\downarrow}$  [10, 21, 35]. By means of elementary integration techniques we get

$$\xi_{BCS}^2 = \frac{\hbar^2}{m\Delta} \frac{[-1 + 2x^2 + 2x\sqrt{1+x^2} - x\pi + 2\operatorname{arcsinh}(x) - 2x\arctan(x) + \ln(4+4x^2)]}{x + \frac{2}{3}x^3 + \frac{2}{3}(1+x^2)^{3/2}}. \quad (46)$$

$$\xi_{\uparrow\downarrow}^2 = \frac{\hbar^2}{4m\Delta} \left[ x + \frac{2+x^2}{(1+x^2)} \left( \frac{\pi}{2} + \arctan(x) \right)^{-1} \right], \quad (47)$$

$$\xi_{\uparrow\uparrow}^2 = \frac{\hbar^2}{8m\Delta} \frac{4 + 3x[\pi + x(2 + \pi x)] + 6(x + x^3)\arctan(x)}{(1+x^2)\left(\frac{\pi}{2} + \arctan(x)\right)}. \quad (48)$$

where  $x = \mu/\Delta$ . These lengths are shown in Fig. 4. It is of interest to explore their asymptotic behavior and compare them with the exponential decay length  $\chi_b$  defined in equation (30). The asymptotic behaviors of  $\xi_{\uparrow\downarrow}$  have been reported in [10] and [35]. On the BCS side we have

$$\begin{aligned}\xi_{\text{BCS}}^2 &\approx \frac{3\hbar^2}{m\epsilon_F}, \\ \xi_{\uparrow\downarrow}^2 &\approx \frac{\hbar^2\epsilon_F}{4m\Delta^2}, \\ \xi_{\uparrow\uparrow}^2 &\approx \frac{3\hbar^2\epsilon_F}{4m\Delta^2}, \\ \chi_b^2 &\approx \frac{\hbar^2\epsilon_F}{m\Delta^2}.\end{aligned}\tag{49}$$

Thus the correlation lengths  $\xi_{\uparrow\downarrow}$  and  $\xi_{\uparrow\uparrow}$  increase in the BCS limit, but are less than  $\chi_b$ , due to spatial oscillations. The mean pair radius  $\xi_{\text{BCS}}$  tends to a finite value that depends only on the density through  $\epsilon_F$ , showing a similar behavior as in 3D [15]. On the BEC side the asymptotic behaviors are

$$\begin{aligned}\xi_{\text{BCS}}^2 &\approx -\frac{\hbar^2}{3m\mu}, \\ \xi_{\uparrow\downarrow}^2 &\approx -\frac{\hbar^2}{3m\mu}, \\ \xi_{\uparrow\uparrow}^2 &\approx -\frac{\hbar^2}{10m}\frac{\Delta^2}{\mu^3}, \\ \chi_b^2 &\approx -\frac{\hbar^2}{4m\mu},\end{aligned}\tag{50}$$

In the 3D system it was found that on the BEC limit  $\xi_{\text{BCS}}^{\text{3D}}$ ,  $\xi_{\uparrow\downarrow}^{\text{3D}}$  and  $\chi_{\text{spec}}^{\text{3D}}$  have the same asymptotic behavior, showing a direct relation with the binding energy of a diatomic molecule [14, 15]. In contrast, in 2D, the lengths  $\xi_{\text{BCS}}$  and  $\xi_{\uparrow\downarrow}$  differ from the exponential decay length  $\chi_b$  of equation (30) by the same numerical factor. Like in 3D, the correlation length  $\xi_{\uparrow\uparrow}$  vanishes faster than the others in the BEC limit. This means Pauli-blocking correlations become negligible, owing to the formation of molecules [14].

## V. DISCUSSIONS AND FINAL REMARKS

We have presented an analysis of the spatial structure of a two-dimensional homogeneous mixture of two fermionic species in the BEC-BCS crossover at the mean-field level with zero temperature. The interspecies pair interaction was modeled by a contact potential. Despite

its simplicity, it introduces divergences, which were removed using two-body scattering physics. Then, the many-body problem becomes dominated by a two-body parameter  $E_a$ . It is important to mention that a scattering length  $a_{2D}$  can be defined with  $E_a$  [2, 26, 37], though we did not consider it explicitly. Our study focuses on three functions: The correlation function of unlike particles  $G_{\uparrow\downarrow}(\mathbf{r})$ , the correlation function of like particles  $G_{\uparrow\uparrow}(\mathbf{r})$ , and the pair wave function  $\phi_{BCS}(\mathbf{r})$ , shown in Fig. 2. These three functions provide a wide image of the spatial structure of the gas throughout the crossover. The pair wave function, being in essence a variational function, determines the behavior of the correlation functions. In the BCS limit, correlated pairs of unlike particles have multiple sizes and Pauli-blocking correlations prevent two like particles to be found near each other. In the BEC limit the localization of the correlation functions indicate that the sizes of correlated pairs of unlike particles tend to be small, while Pauli-blocking correlations become negligible. These features can be seen explicitly thanks to our analytical expressions of the two correlation functions, see equations (21), (22), (28), and (29). These expressions are in good agreement with the asymptotic behaviors already reported in the literature [38]. For example, we can see that the correlation function of unlike particles  $\uparrow\downarrow$  exhibits a logarithmic divergence multiplied by Tan's contact at short distances [2, 38, 39], see equation (28). With the aid of our analytical expressions, we were able to study the large-distance behavior of the two correlation functions and the pair wave function, where we found a well-defined oscillatory behavior and an exponential decay. The large-distance oscillations of the three functions are characterized by the Fermi wave number  $k_F$  throughout the crossover. This behavior differs from the 3D case [14], where the oscillation wave vectors decrease as we approach the BEC limit, with the disappearance of the Fermi-surface. We believe an explanation of this behavior in 2D requires further considerations, such as the use of a finite range interaction, instead of the contact interaction [40, 41], and the inclusion of beyond mean-field corrections. The phase differences between the three functions show that their nodes (or maximums also) form a structure of concentric circles. In contrast with 3D, the positions of the nodes of the correlation functions never change throughout the crossover. However, the nodes of the pair wave function move from the zeros of  $J_2(k_F r)$ , in the BCS limit, to the zeros of  $J_0(k_F r)$ , in the BEC limit. For the exponential decay behavior we found the three functions have the same exponential decay length  $\chi_b$ , see equation (30), which is a length associated to the two-body parameter  $E_a$ . Thus, in 2D, the exponential decay is explicitly determined by

the two-body physics introduced to renormalize the interaction strength  $g$ . Comparing the behavior of the exponential decay length in 2D with its analogue in 3D, shown in equation (44), we conclude that the threshold energy  $\epsilon_{\text{spec}}$ , see equation (11), gives the exponential decay length in 2D and in 3D. A compact way to access the information contained in the correlation functions and the pair wave function is by their respective second moments, which are called correlation lengths and mean pair radius, see equation (45). Nevertheless, we have shown that the information about the large-distance structure is quiet diluted in these lengths. We found that they behave similarly to their analogues in 3D [10, 15, 42]. In the BCS limit the correlation lengths diverge, while the mean pair radius is finite. In the BEC limit the three lengths vanish in the BEC side. However, a difference with 3D is that in 2D the correlation length of unlike species  $\xi_{\uparrow\downarrow}$  and the mean pair radius  $\xi_{\text{BCS}}$  are not strictly equal to the exponential decay length  $\chi_b$  in the BEC limit. As an extension of this work, it will be of interest to study the large distance behavior of the correlation functions in quasi-2D geometries, which are of current interest for understanding the evolution from 3D to 2D [2]. Also, it is of interest to see how the large-distance properties are modified by beyond mean-field corrections, and the use of a short-range potential [36, 40, 41, 43–46].

## ACKNOWLEDGMENTS

We thank support from UNAM PAPIIT-IN108620. J.C.O.-J. acknowledges support from a CONACYT scholarship.

## Appendix A: Inverse Fourier transforms of $g_{\uparrow\downarrow}(r)$ and $g_{\uparrow\uparrow}(r)$

The inverse Fourier transform of  $g_{\uparrow\downarrow}(r)$  can be written in the following way:

$$\int d^2r e^{-i\mathbf{k}\cdot\mathbf{r}} g_{\uparrow\downarrow}(r) = \frac{(2\pi)}{k_F^2} \int_0^\infty g_{\uparrow\downarrow}(\rho) \rho J_0(\kappa\rho) d\rho, \quad (\text{A1})$$

where we made a transformation to polar coordinates and evaluated the angular integral, which allows us to identify the integral representation of the Bessel function of the first kind of order zero  $J_0(\kappa\rho)$  (27). Also, we scaled variables with the Fermi wave number  $k_F$ , such that  $\rho = k_F r$  and  $\kappa = k/k_F$ , where  $k = |\mathbf{k}|$ . Substituting the explicit form of  $g_{\uparrow\downarrow}(r)$  given in

equation (28) we get

$$\int d^2r e^{-i\mathbf{k}\cdot\mathbf{r}} g_{\uparrow\downarrow}(r) = \frac{\tilde{\Delta}}{2} \int_0^\infty \rho J_0(\rho) K_0\left(\frac{\rho}{\sqrt{2}k_F\chi_b}\right) J_0(\kappa\rho) d\rho \quad (\text{A2})$$

The integral on the right side of equation (A2) has been evaluated and can be found in a table of integrals, like [33] or [32]. Here we write the general expression:

$$\int_0^\infty x J_0(ax) K_0(bx) J_0(cx) dx = [a^4 + b^4 + c^4 - 2a^2c^2 + 2a^2b^2 + 2b^2c^2]^{-1/2} \quad (\text{A3})$$

where  $\text{Re } b > |\text{Im } a|$  and  $c > 0$ . With the identification of  $a = 1$ ,  $b = \{[(\tilde{\mu}^2 + \tilde{\Delta}^2)^{1/2} - \tilde{\mu}]/2\}^{1/2}$ , and  $c = \kappa$ , together with the aid of equations (10) and (12), we get the desired result:

$$\int d^2r e^{-i\mathbf{k}\cdot\mathbf{r}} g_{\uparrow\downarrow}(r) = \frac{\tilde{\Delta}}{2\sqrt{(\kappa^2 - \tilde{\mu})^2 + \tilde{\Delta}^2}} = v_k u_k. \quad (\text{A4})$$

In a similar way, we find the inverse Fourier transform of  $g_{\uparrow\uparrow}(r)$  to be given by

$$\int d^2r e^{-i\mathbf{k}\cdot\mathbf{r}} g_{\uparrow\uparrow}(r) = \frac{\tilde{\Delta}}{2} \int_0^\infty K_1\left(\frac{\rho}{\sqrt{2}k_F\chi_b}\right) J_1(\rho) \rho J_0(\kappa\rho) d\rho. \quad (\text{A5})$$

The integral on the right side can be identified as a particular case of a great variety of integrals, see for instance [33] and [32]. However, not all the expressions are adequate for the purpose of identifying  $v_k^2$ . Thus, we will give a sketch of how to prove that the right side of equation (A5) is  $v_k^2$ . We can start with the following general integral [32, 33]:

$$\int_0^\infty x^{\nu+1} K_\mu(ax) I_\mu(bx) J_\nu(cx) dx = \frac{(ab)^{-\nu-1} c^\nu e^{-(\nu+1/2)\pi i} Q_{\mu-1/2}^{\nu+1/2}(u)}{\sqrt{2\pi}(u^2 - 1)^{\frac{1}{2}\nu + \frac{1}{4}}} \quad (\text{A6})$$

where  $u = (a^2 + b^2 + c^2)/(2ab)$ , with  $\text{Re } a > |\text{Re } b| + |\text{Im } c|$ ,  $\text{Re } \nu > -1$  and  $\text{Re}(\mu + \nu) > -1$ . In this equation  $I_\mu$  is the modified Bessel function of the first kind of order  $\mu$  and  $Q_\alpha^\beta$  is an associated Legendre function of the second kind. The values of the constants we are interested in are  $a = \{[(\tilde{\mu}^2 + \tilde{\Delta}^2)^{1/2} - \tilde{\mu}]/2\}^{1/2}$ ,  $b = i$  and  $c = \kappa$ , while the subscripts are  $\mu = 1$  and  $\nu = 0$ . The associated Legendre function of the second kind can be expressed in terms of the hypergeometric function  ${}_2F_1$  in the following way [31, 33]:

$$Q_\alpha^\beta(z) = \frac{e^{\beta\pi i}}{2^{\alpha+1}} \frac{\Gamma(\alpha + \beta + 1)}{\Gamma(\alpha + 3/2)} \frac{\Gamma(1/2)(z^2 - 1)^{\beta/2}}{z^{\alpha+\beta+1}} {}_2F_1\left(\frac{\alpha + \beta}{2} + 1, \frac{\alpha + \beta + 1}{2}; \alpha + \frac{3}{2}, \frac{1}{z^2}\right), \quad (\text{A7})$$

where  $\Gamma$  is the well-known Gamma function. Finally, we also need an integral representation of the hypergeometric function [31, 33]:

$${}_2F_1(\alpha, \beta, \gamma; z) = \frac{1}{B(\beta, \gamma - \beta)} \int_0^1 t^{\beta-1} (1-t)^{\gamma-\beta-1} (1-tz)^{-\alpha} dt, \quad (\text{A8})$$

where  $\text{Re } \gamma > \text{Re } \beta > 0$ , and  $B$  is the beta function. For our particular case, the integral in equation (A8) can be evaluated by elementary integration techniques. Hence, we can substitute equations (A7) and (A8) into (A6) to obtain

$$\int_0^\infty x K_1\left(\frac{x}{\sqrt{2}k_F\chi_b}\right) I_1(ix) J_0(\kappa x) dx = \frac{1}{i2\sqrt{(1-\tilde{\mu})}} \left( \frac{1}{\left(1 - \frac{1}{u^2}\right)^{1/2}} - 1 \right), \quad (\text{A9})$$

where  $u = (\kappa^2 - \tilde{\mu})/(2i\sqrt{1-\tilde{\mu}})$  and we expressed the gap  $\tilde{\Delta}$  in terms of the chemical potential  $\tilde{\mu}$  using equations (10) and (12). From equation (A9) we can identify the right side of equation (A5) recalling that  $I_\nu(x) = e^{-\nu\pi i/2} J_\nu(e^{i\pi/2}x)$ . After some rearrangements we conclude that

$$\int d^2r e^{-i\mathbf{k}\cdot\mathbf{r}} g_{\uparrow\uparrow}(r) = v_k^2. \quad (\text{A10})$$

## Appendix B: Large-distance approximation of the pair wave function

Introducing the approximation of the Bessel function  $J_0(kr)$ , given in equation (38), into equation (26) we have

$$\phi_{\text{BCS}}(r) \approx \frac{k_\Delta^{3/2}}{\sqrt{2\pi^3 r}} \left[ \frac{S_1(r)e^{-i\pi/4} + S_2(r)e^{i\pi/4}}{2} \right], \quad (\text{B1})$$

where we scaled the lengths with the wave vector  $k_\Delta$  associated to the gap  $\Delta = \hbar^2 k_\Delta^2 / 2m$  and defined

$$S_1(r) = \int_0^\infty \sqrt{p} \mathcal{F}(p) e^{ipk_\Delta r} dp \quad (\text{B2})$$

$$S_2(r) = \int_0^\infty \sqrt{p} \mathcal{F}(p) e^{-ipk_\Delta r} dp. \quad (\text{B3})$$

For the pair wave function we have

$$\mathcal{F}(p) = \sqrt{(p^2 - \mu_\Delta)^2 + 1} - (p^2 - \mu_\Delta), \quad (\text{B4})$$

where  $\mu_\Delta = \mu/\Delta$ . Using the change of variable  $p = e^{i\pi/2}x$  in  $S_1(r)$  and  $p = e^{-i\pi/2}x$  in  $S_2(r)$  we get

$$\phi_{\text{BCS}}(r) \approx -\frac{ik_\Delta^{3/2}}{2^{3/2}\sqrt{\pi^3 r}} \left[ \int_{\mathbb{I}} \sqrt{x} \mathcal{F}(ix) e^{-xk_\Delta r} dx \right], \quad (\text{B5})$$

where the integral is over the imaginary axis, from  $x = -i\infty$  to  $x = i\infty$ . The integrand has five branch cuts, see equations (B4) and (B5). Four of them are determined by the equations:

$$\operatorname{Re}[(x^2 + \mu_\Delta)^2 + 1] \leq 0, \text{ and } \operatorname{Im}[(x^2 + \mu_\Delta)^2 + 1] = 0. \quad (\text{B6})$$

Using  $x = a + ib$  we find that those branch cuts correspond to points in the hyperbola  $b^2 - a^2 = \mu_\Delta$  whose magnitude satisfies  $|x|^2 \geq (\mu_\Delta^2 + 1)^{1/2}$ . As the integrand in the right side of equation (B5) decreases exponentially when  $\operatorname{Re} x \rightarrow \infty$ , we can close a contour to the right side of the complex plane with a semicircle-like contour, which surrounds infinitesimally two branch cuts. We illustrate this contour in Fig. 5

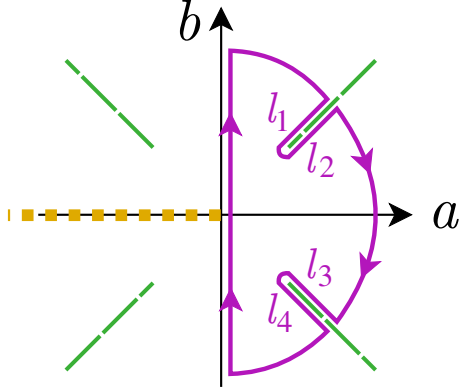


FIG. 5. (Color online) Illustration of the branch cuts of the integrand in equation (B5). The large dashes (green) correspond to the branch cuts of  $\mathcal{F}(ix)$ , see equation (B4), while the short dashes (orange) to the branch cut of  $\sqrt{x}$ . The solid line (purple) is the contour used in the Cauchy's integral formula in equation (B7). Close to the branch cuts we have four paths denoted by  $l_i$ , with  $i = 1, 2, 3, 4$ .

From Cauchy's integral formula we have [34]

$$\oint_{\mathcal{C}} \sqrt{x} \mathcal{F}(ix) e^{-xk_\Delta r} dx = 0, \quad (\text{B7})$$

where  $\mathcal{C}$  is the contour shown in Fig. 5. Taking the radius of the semicircle to infinity, we

get

$$\begin{aligned} \int_{\mathbb{I}} \sqrt{x} \mathcal{F}(ix) e^{-xk_{\Delta}r} dx &= 2 \int_{l_2} \sqrt{x} \sqrt{|(x^2 + \mu_{\Delta})^2 + 1|} e^{-i\pi/2} e^{-xk_{\Delta}r} dx \\ &\quad + 2 \int_{l_4} \sqrt{x} \sqrt{|(x^2 + \mu_{\Delta})^2 + 1|} e^{-i\pi/2} e^{-xk_{\Delta}r} dx, \end{aligned} \quad (\text{B8})$$

where  $l_2$  and  $l_4$  are the trajectories depicted in Fig. 5. The parametrization of  $l_2$  is given by  $\gamma_2(t) = t + i(t^2 + \mu_{\Delta})^{1/2}$ , while the parametrization of  $l_4$  is  $\gamma_4(t) = t - i(t^2 + \mu_{\Delta})^{1/2}$ , with  $t \in [t_0, \infty)$ , where

$$t_0 = \left( \frac{(\mu_{\Delta}^2 + 1)^{1/2} - \mu_{\Delta}}{2} \right)^{1/2}. \quad (\text{B9})$$

With the explicit form of the parametrizations we can join the two integrals in equation (B8) in the following way:

$$\int_{\mathbb{I}} \sqrt{x} \mathcal{F}(ix) e^{-xk_{\Delta}r} dx = 4 \int_{t_0}^{\infty} \sqrt{4t^2(t^2 + \mu_{\Delta}) - 1} e^{-i\pi/2} e^{-tk_{\Delta}r} \operatorname{Re}[e^{-i\sqrt{t^2 + \mu_{\Delta}}} \sqrt{\gamma_2(t)} \gamma_2'(t)] dt. \quad (\text{B10})$$

To get an explicit expression we can notice that the branch cuts always remain in their own quadrant. Then with de Moivre's formula the parametrization can be written as

$$\gamma_2(t) = (2t^2 + \mu_{\Delta})^{1/2} [\cos \theta(t) + i \sin \theta(t)], \quad (\text{B11})$$

where we have defined

$$\theta(t) = \arctan \left( \frac{\sqrt{t^2 + \mu_{\Delta}}}{t} \right). \quad (\text{B12})$$

This form helps us to calculate  $\sqrt{\gamma_2(t)}$  in equation (B10). Then we get explicitly

$$\begin{aligned} \int_{\mathbb{I}} \sqrt{x} \mathcal{F}(ix) e^{-xk_{\Delta}r} dx &= 4 \int_{t_0}^{\infty} \sqrt{4t^2(t^2 + \mu_{\Delta}) - 1} e^{-i\pi/2} e^{-tk_{\Delta}r} (2t^2 + \mu_{\Delta})^{1/4} \\ &\quad \times \left\{ \cos(\sqrt{t^2 + \mu_{\Delta}}) \left[ \cos(\theta(t)/2) - \frac{t \sin(\theta(t)/2)}{\sqrt{t^2 + \mu_{\Delta}}} \right] \right. \\ &\quad \left. + \sin(\sqrt{t^2 + \mu_{\Delta}}) \left[ \frac{t \cos(\theta(t)/2)}{\sqrt{t^2 + \mu_{\Delta}}} + \sin(\theta(t)/2) \right] \right\} dt. \end{aligned} \quad (\text{B13})$$

Substituting equation (B13) into equation (B5) and scaling variables with  $k_F$  instead of  $k_{\Delta}$  we obtain equation (39).

---

[1] T. Hazra, N. Verma, and M. Randeria, Phys. Rev. X **9**, 031049 (2019).

[2] J. Levinsen and M. M. Parish, “Strongly interacting two-dimensional fermi gases,” in *Annual Review of Cold Atoms and Molecules*, Chap. 1, pp. 1–75.

[3] W. Ketterle and M. W. Zwierlein, Riv. Nuovo Cimento **164**, 95 (2008).

[4] G. C. Strinati, P. Pieri, G. Röpke, P. Schuck, and M. Urban, Physics Reports **738**, 1 (2018).

[5] I. Bloch, J. Dalibard, and W. Zwerger, Rev. Mod. Phys. **80**, 885 (2008).

[6] P. Dyke, E. D. Kuhnle, S. Whitlock, H. Hu, M. Mark, S. Hoinka, M. Lingham, P. Hannaford, and C. J. Vale, Phys. Rev. Lett. **106**, 105304 (2011).

[7] A. T. Sommer, L. W. Cheuk, M. J. H. Ku, W. S. Bakr, and M. W. Zwierlein, Phys. Rev. Lett. **108**, 045302 (2012).

[8] M. Feld, B. Fröhlich, E. Vogt, M. Koschorreck, and M. Köhl, Nature **480**, 75 (2011).

[9] K. Miyake, Progress of Theoretical Physics **69**, 1794 (1983).

[10] M. Randeria, J.-M. Duan, and L.-Y. Shieh, Phys. Rev. B **41**, 327 (1990).

[11] A. J. Leggett, in *Modern Trends in the Theory of Condensed Matter* (Springer Berlin Heidelberg, Berlin, Heidelberg, 1980) pp. 13–27.

[12] D. M. Eagles, Phys. Rev. **186**, 456 (1969).

[13] J. Bardeen, L. N. Cooper, and J. R. Schrieffer, Phys. Rev. **108**, 1175 (1957).

[14] J. C. Obeso-Jureidini and V. Romero-Rochín, Phys. Rev. A **101**, 033619 (2020).

[15] G. Ortiz and J. Dukelsky, Phys. Rev. A **72**, 043611 (2005).

[16] L. D. Landau and E. M. Lifshitz, *Quantum mechanics: non-relativistic theory*, Vol. 3 (Elsevier, 2013).

[17] S. K. Adhikari, American Journal of Physics **54**, 362 (1986), <https://doi.org/10.1119/1.14623>.

[18] I. R. Lapidus, American Journal of Physics **50**, 45 (1982), <https://doi.org/10.1119/1.13004>.

[19] L. Salasnich and F. Toigo, Physics Reports **640**, 1 (2016), zero-point energy of ultracold atoms.

[20] S. A. Morgan, M. D. Lee, and K. Burnett, Phys. Rev. A **65**, 022706 (2002).

[21] M. Marini, F. Pistolesi, and G. Strinati, The European Physical Journal B - Condensed Matter and Complex Systems **1**, 151 (1998).

[22] L. Salasnich, Phys. Rev. A **76**, 015601 (2007).

[23] S.-L. Nyeo, American Journal of Physics **68**, 571 (2000), <https://doi.org/10.1119/1.19485>.

[24] M. Tinkham, *Introduction to Superconductivity*, Dover Books on Physics Series (Dover Publications, 2004).

[25] V. Romero-Rochín, Journal of Physics B: Atomic, Molecular and Optical Physics **44**, 095302

(2011).

- [26] L. Salasnich and F. Toigo, Phys. Rev. A **91**, 011604 (2015).
- [27] C. H. Schunck, Y.-i. Shin, A. Schirotzek, and W. Ketterle, Nature **454**, 739 (2008).
- [28] L. D. Landau and E. Lifshitz, *Statistical Physics, Part 1*, Vol. 5 (Butterworth-Heinemann, 1980).
- [29] S. Giorgini, L. P. Pitaevskii, and S. Stringari, Rev. Mod. Phys. **80**, 1215 (2008).
- [30] A. M. Kadin, Journal of superconductivity and novel magnetism **20**, 285 (2007).
- [31] H. Bateman, A. Erdélyi, W. Magnus, F. Oberhettinger, and F. G. Tricomi, *Higher transcendental functions* (McGraw-Hill, New York, 1953) volumes I and II.
- [32] H. Bateman, A. Erdélyi, W. Magnus, F. Oberhettinger, and F. G. Tricomi, *Tables of integral transforms*, Vol. II (McGraw-Hill Book Company, New York, 1954).
- [33] I. Gradshteyn and I. Ryzhik, *Table of integrals, series, and products*, edited by D. Zwillinger and V. Moll (Academic press, 2014).
- [34] J. Marsden and M. Hoffman, *Basic Complex Analysis* (W. H. Freeman, New York, 1999).
- [35] M. Casas, J. M. Getino, M. de Llano, A. Puente, R. M. Quick, H. Rubio, and D. M. van der Walt, Phys. Rev. B **50**, 15945 (1994).
- [36] F. Marsiglio, P. Pieri, A. Perali, F. Palestini, and G. C. Strinati, Phys. Rev. B **91**, 054509 (2015).
- [37] C. Mora and Y. Castin, Phys. Rev. A **67**, 053615 (2003).
- [38] F. Werner and Y. Castin, Phys. Rev. A **86**, 013626 (2012).
- [39] S. Tan, Annals of Physics **323**, 2971 (2008).
- [40] M. M. Parish, B. Mihaila, E. M. Timmermans, K. B. Blagoev, and P. B. Littlewood, Phys. Rev. B **71**, 064513 (2005).
- [41] E. Neri, S. F. Caballero-Benítez, V. Romero-Rochín, and R. Paredes, Physica Scripta **95**, 034013 (2020).
- [42] F. Palestini and G. C. Strinati, Phys. Rev. B **89**, 224508 (2014).
- [43] S. F. Caballero-Benítez, R. Paredes, and V. Romero-Rochín, Physics Letters A **377**, 1756 (2013).
- [44] G. Bighin and L. Salasnich, International Journal of Modern Physics B **32**, 1840022 (2018).
- [45] G. Bighin and L. Salasnich, Phys. Rev. B **93**, 014519 (2016).
- [46] L. He, H. Lü, G. Cao, H. Hu, and X.-J. Liu, Phys. Rev. A **92**, 023620 (2015).